scientific reports

Check for updates

OPEN

Assessing the effectiveness of vegetation indices in detecting forest disturbances in the southeast Amazon

Eduardo Q. Marques[1,2,3]✉, Divino V. Silvério[1,3], Lenio S. Galvão[4], Luiz E. O. C. Aragão[4], Maria R. Uribe[5], Marcia N. Macedo[2,6], Ludmila Rattis[2,6], Ane A. C. Alencar[2] & Paulo M. Brando[2,5]

Amazon forests are becoming increasingly vulnerable to disturbances such as droughts, fires, windstorms, logging, and forest fragmentation, all of which lead to forest degradation. Nevertheless, quantifying the extent and severity of disturbances and their cumulative impact on forest degradation remains a significant challenge. In this study, we combined multispectral data from Landsat sensors with hyperspectral data from the Earth Observing-One (Hyperion/EO-1) sensor to evaluate the efficacy of multiple vegetation indices in detecting forest responses to disturbances in an experimentally burned forest in southeastern Amazonia. Our experimental area was adjacent to an agricultural field and consisted of three 50-ha treatments – an unburned Control, a plot burned every three years, and a plot burned annually from 2004 to 2010. All plots were monitored to assess vegetation recovery after fire disturbance. These areas were also affected by three drought events (2007, 2010, and 2016) over the study period. We evaluated a total of 18 Vegetation Indices (VI), one unique to Landsat, 12 unique to Hyperion/EO-1, and five commons to both satellites (i.e., 6 total from Landsat and 17 from Hyperion). We used linear models (LM) to evaluate how changes in ground observations of forest structure (biomass, leaf area index [LAI], and litter production) associated with fire were captured by the two VIs most sensitive to forest degradation. Our results indicate that the Plant Senescence Reflectance Index (PSRI) derived from Hyperion/EO-1 was the most sensitive to vegetation changes associated with forest fires, increasing by 94% in burned vs. unburned forests. Of the Landsat-derived VIs, we found that the Green-Red Normalized Difference (GRND) were the most sensitive to forest degradation by fire, showing a marked decline (87%) in the burned plots compared with the unburned Control. However, compared to PSRI, the GRND was a better predictor of changes associated with fire, both in the forest interior or forest edge, for the three ground variables: biomass stocks ($r^2 = 0.5–0.8$), LAI ($r^2 = 0.8–0.9$), and litter production ($r^2 = 0.4–0.7$). This study demonstrate that VIs can detect forest responses to fire and other disturbances over time, highlighting the relative strengths of each VI. In doing so, it shows how the integration of multispectral and hyperspectral data can be useful for monitoring tropical forest degradation and recovery. Moreover, it provides valuable insights into the limitations of existing approaches, which can inform the design of next-generation sensors for global forest monitoring.

Keywords Remote sensing, Satellite imagery, Spectral response, Hyperion, Forest degradation, Disturbance

Tropical regions face unprecedented exposure to disturbances from logging, fires, forest fragmentation, and climate change, often accelerating the pace and extent of forest degradaton[1]. Forest degradation refers to the decline in the ecological quality and functionality of a forest, which occurs as a result of disturbances such as biodiversity loss, reduction in forest structure, and diminished ecosystem services[2]. Recent studies in southeastern

[1]Universidade do Estado de Mato Grosso, Nova Xavantina, MT, Brazil. [2]Instituto de Pesquisa Ambiental da Amazônia, Brasília, DF, Brazil. [3]Universidade Federal Rural da Amazônia, Capitão Poço, PA, Brazil. [4]Instituto Nacional de Pesquisas Espaciais, São José dos Campos, SP, Brazil. [5]Yale School of the Environment, Yale University, Yale, CT, USA. [6]Woodwell Climate Research Center, Falmouth, MA, USA. ✉email: eduardo.marques@unemat.br

Amazonia have shown that forest fires, fragmentation, and climate extremes have reduced the ability of forests to store and accumulate carbon[3,4]. As deforestation and the accumulation of atmospheric greenhouse gases (GHGs) alter the region's climate, such disturbances will likely affect large swaths of the Amazon. For instance, forest fires could affect about 16% of these forests by 2050[5]. However, detailed mapping of forest degradation from multiple disturbances is rare, making it difficult to quantify their effects on ecosystem processes and create effective monitoring systems to track forest integrity[6–9].

Some estimates show that forest degradation in recent decades may have surpassed forest deforestation, showing the urgency of quantifying the severity and extent of forest degradation in the Amazon. Between 1992 and 2014, forest degradation in the Brazilian Amazon associated with fire, logging, and fragmentation affected an area of 337 thousand km^2, surpassing deforestation during the same period (308 thousand km^2)[10]. Hence, it is imperative to enhance the mapping and monitoring of forest degradation in the Amazon, despite the existence of numerous technical obstacles[11]. First, forest disturbances vary widely in intensity and severity, ranging from complete loss of the forest canopy to varying degrees of forest degradation[10]. Although high-severity disturbances (e.g., deforestation) are easily detected using standard remote sensing techniques[11], mapping small-scale cryptic disturbances is far more challenging. Moreover, Amazonian forests vary in structure, function, and diversity, posing additional challenges for identifying disturbances that cause forest degradation[12]. Despite these and other difficulties, recent advances in satellite data represent new opportunities for mapping forest degradation over time[13].

The Landsat time series is among the most important tools for mapping temporal and spatial patterns of deforestation and forest degradation. Landsat sensors such as the Operational Land Imager (OLI) and Thematic Mapper (TM) have provided images at 30-m spatial resolution since 1984, which is by far the most comprehensive time series for monitoring tropical deforestation[14,15]. However, their low temporal (16 days) and spectral resolutions have limited ability to quantify the severity and extent of forest degradation[16]. This is partly because commonly used vegetation indices (VIs) tend to saturate as the forest canopy closes following disturbance. Given the rapid recovery of foliage after a disturbance event, traditional multispectral indices may not be sufficiently sensitive to monitor the impacted areas with longer recovery times[6].

The need to identify finer-scale patterns of forest degradation is clear in recent literature[10,17]. Achieving this requires the use of advanced satellite technologies that improve both spatial and spectral resolutions[18]. In November 2000, the National Aeronautics and Space Administration (NASA) launched the Hyperion spaceborne sensor onboard the Earth Observing (EO-1) satellite. Hyperion was a hyperspectral mission that obtained images in 242 contiguous narrow bands (198 radiometrically calibrated bands) covering the 400 to 2,500 nm spectral interval[6,13], with a swath width of 7.7 km and 30 m spatial resolution. Despite being discontinued in 2017, the archive of historical Hyperion images offers valuable insights for tracking forest degradation, which may surpass the capabilities of current Landsat instruments[13]. Moreover, the use of Hyperion data offers an opportunity to develop studies that may help designing newer hyperspectral sensor missions, with even better technical specifications than Hyperion[19]. Hyperspectral imagery may help improve our ability to detect disturbance-driven changes in forest structure (e.g., leaf area index and aboveground biomass), productivity (e.g., litter and wood increment), and diversity (e.g., species richness and composition).

Combining multispectral (Landsat TM and OLI) and hyperspectral (Hyperion) data provides an opportunity to better quantify forest degradation in response to the understory fire resilience capacity to recover after disturbance, which is challenging in the Amazon. Datasets from controlled burn experiments offer unique research opportunities for tracking forest degradation caused by fires as well as the use of VIs as indicators of forest recovery over time. One such experiment, performed over a forest fragment at Tanguro farm (Mato Grosso state, Brazil) from 2004 to 2010, included an unburned plot Control, a plot burned every year, and a plot burned every three years[20]. Using the time series of multispectral and hyperspectral data measured over these plots, together with field data collected throughout the experiment, enabled us to test the efficacy of VIs for detecting forest degradation by fire.

In this study, we used multispectral data from the Landsat satellite (TM and OLI) and hyperspectral data from the EO-1 satellite (Hyperion) to determine the VIs most sensitive to forest degradation caused by experimental fires in the southern Amazon, which co-occurred with droughts, windstorms, and along the forest edge. Specifically, we investigated the following questions: (1) What spectral changes in vegetation are detectable by VIs after a fire event? (2) How can the use of hyperspectral images improve our ability to map and quantify forest degradation caused by fires and edge effects? (3) Which VIs best capture changes in forest structure and productivity associated with fires and the capacity of forests to recover from this disturbance?

Materials and methods

Study area and datasets

Our study area is in the municipality of Querência (Mato Grosso state) in the southeastern portion of the Amazon Basin (13°04′35.39" S, 52°23′08.85" W). The climate of the region is tropical with a dry winter (Aw), according to the Köppen classification, with well-defined dry (May to September) and rainy (October to April) periods[21]. The experimental area was described in detail by Balch et al. (2008)[20]. Briefly, the experimental area comprised three adjacent plots of 50 ha each, each subject to different burning regimes: an unburned (Control), a plot burned every year (B1 year), and a plot burned every three years (B3 year) from 2004 to 2010, except for 2008 (Fig. 1). During this period, the B3 year and B1 year plots were burned three and six times, respectively[22]. All plots have been monitored continuously since the last fire in 2010 to track forest recovery over time.

To calculate the aboveground biomass (AGB), we conducted forest inventories for all experimental plots from 2004 to 2017. Leaf Area Index (LAI) was measured at multiple points in each plot from 2005 to 2017. Litterfall production was monitored from 2004 to 2018, using 210 baskets (70 per plot). These field observations

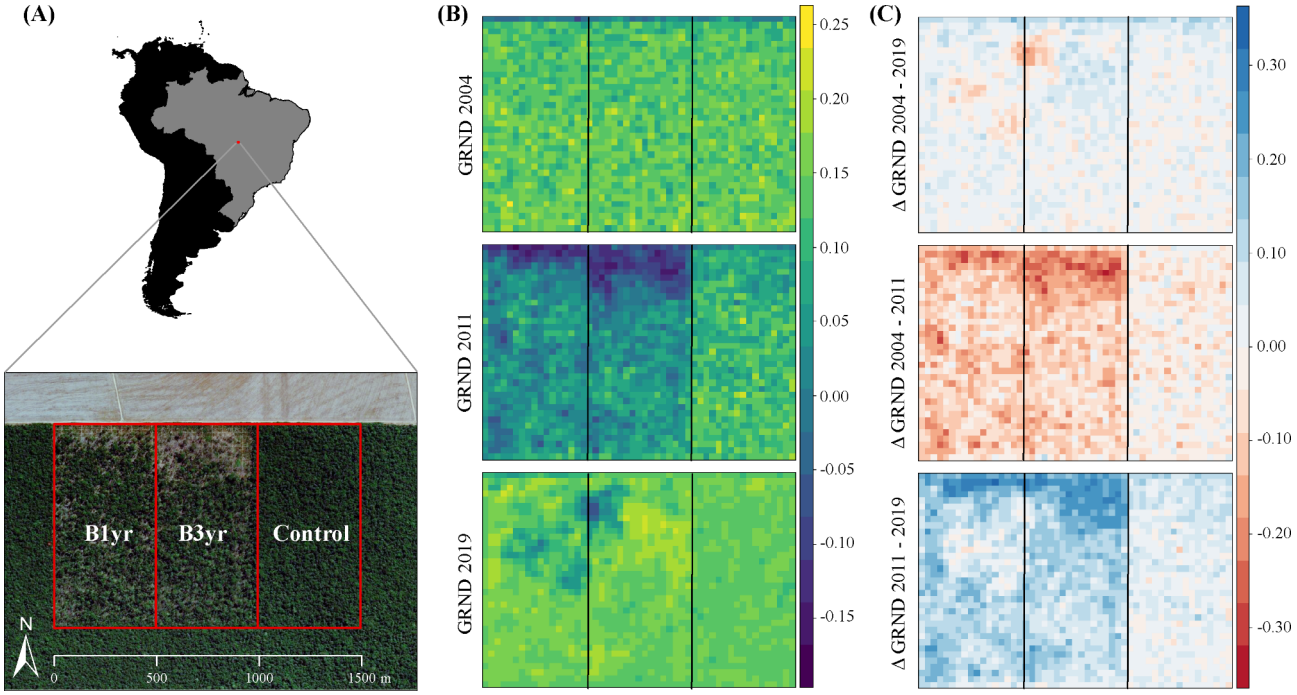

Fig. 1. (**A**) Location of experimental fire plots in southern Amazonia. (**B**) Green-Red Normalized Difference (GRND), a VI calculated from Landsat data that is sensitive to greenness. The results are presented for three periods: before the fire experiment (2004), after the last fire (2011), and after eight years of vegetation recovery (2019). (**C**) Delta GRND, calculated for these three periods to quantify differences associated with repeated fires (Δ 2004–2011); post-fire vegetation recovery (Δ 2011–2019); and the proportion of vegetation recovery relative to the baseline (Δ 2004–2019).

were then used to assess correlations with satellite-based VIs. Detailed information is available in Appendix S1: Sect. 1.

We used 45 TM/Landsat-5 and 22 OLI/Landsat-8 images from 1985 to 2019 to analyze changes in vegetation after forest disturbance. For each year, we calculated six VIs from the available Landsat data. In addition, we used Hyperion/EO-1 data from 2004 to 2012 to compute 17 VIs and assess their sensitivity to vegetation degradation after the experimental fires. We used images from the dry season (June to August) to mitigate potential biases owing to the influence of seasonal variations on our analysis. Detailed equations and references for the calculated VIs are listed in Table 1. Both the Landsat and EO-1 images came from the USGS and underwent atmospheric and geometric corrections. Further information regarding pre-processing and corrections for each set of satellite images can be found in Appendix S1: Sect. 1.

Data analysis

To assess the efficacy of each VI in detecting post-fire vegetation changes, we calculated the percentage spectral change over the study area. The efficacy of each VI in detecting fire-associated changes was calculated as the difference between the values in the burned plots (B1 year and B3 year) and the Control plot, and then standardized as a percentage. We then evaluated the uncertainties by calculating 95% confidence intervals based on the 'Z' distribution test to compare across the treatments. To evaluate the variability of the multispectral VIs over time and the differences between treatments, we generated a simple model of temporal change by employing the Loess method as implemented in the *geom_smooth* function of the R package *ggplot2*[23]. We also incorporated the standard errors (SE), calculated based on the Loess methods, to better assess the model's precision and improve confidence in its predictions[24]. For the hyperspectral VIs, we employed the same method to evaluate the differences between plots; however, the analysis was restricted to the indices that showed the strongest responses to forest disturbances. To evaluate vegetation response to edge effects, we compared the responses of multispectral and hyperspectral VIs at the forest edge (first 250 m) to the forest interior (> 250 m from the edge) of the experimental plot.

To assess how hyperspectral images improve our ability to map and understand forest degradation, we performed Principal Component Analyses (PCA) for the entire hyperspectral time series (2004–2012) and for individual years, allowing us to identify patterns of vegetation change throughout the fire experiment. For annual PCAs, we compared the pre-experiment (2004) and post-experiment (2012) periods. We then used eigenvectors to evaluate the relative contribution of each VI to the explanation of a given component. We also compared the results of the 17 hyperspectral VIs with those of the six multispectral VIs using Pearson's correlation coefficients to develop a correlation matrix, which enabled us to verify which hyperspectral VIs were mostly correlated with the multispectral VIs (≥ 0.9).

Vegetation index	Equation	Satellite
Structure		
Enhanced vegetation index (EVI)	$2.5\times((\rho 864nm-\rho 660nm)/(\rho 864nm+6\times\rho 660nm-7.5\times\rho 467nm+1))$	Landsat, Hyperion
Normalized difference vegetation index (NDVI)	$(\rho 864nm-\rho 660nm)/(\rho 864nm+\rho 660nm)$	Landsat, Hyperion
Visible atmospherically resistant index (VARI)	$(\rho 559nm-\rho 660nm)/(\rho 559nm+\rho 660nm\text{-}\rho 487nm)$	Hyperion
Visible index green (VIG)	$(\rho 559nm-\rho 660nm)/(\rho 559nm+\rho 660nm)$	Hyperion
Green-red normalized difference (GRND)	$(\rho 560nm-\rho 660nm)/(\rho 560nm+\rho 660nm)$	Landsat
Biochemistry		
Leaf water vegetation index2 (LWVI2)	$(\rho 1094nm-\rho 1205nm)/(\rho 1094nm+\rho 1205nm)$	Hyperion
Moisture stress index (MSI)	$(\rho 1598nm)/(\rho 823nm)$	Hyperion
Normalized difference infrared index (NDII)	$(\rho 823nm-\rho 1649nm)/(\rho 823nm+\rho 1649nm)$	Landsat, Hyperion
Normalized difference water index (NDWI)	$(\rho 854nm-\rho 1245nm)/(\rho 854nm+\rho 1245nm)$	Hyperion
Pigment specific simple ratio (PSSR)	$(\rho 803nm)/(\rho 671nm)$	Hyperion
Plant senescence reflectance index (PSRI)	$(\rho 681nm\text{-}\rho 498nm)/(\rho 752nm)$	Hyperion
Structure insensitive pigment index (SIPI)	$(\rho 803nm-\rho 467nm)/(\rho 803nm+\rho 681nm)$	Hyperion
Water band index (WBI)	$(\rho 905nm)/(\rho 972nm)$	Hyperion
Near-infrared reflectance of vegetation (NIRv)	$(\rho 864nm)\times((\rho 864nm-\rho 660nm)/(\rho 864nm+\rho 660nm))$	Hyperion
Physiology		
Photochemical reflectance index (PRI)	$(\rho 529nm-\rho 569nm)/(\rho 529nm+\rho 569nm)$	Hyperion
RedEdge NDVI (RENDVI)	$(\rho 752nm-\rho 701nm)/(\rho 752nm+\rho 701nm)$	Hyperion
Fire		
Normalized burn ratio (NBR)*	Hyperion = $(\rho 823nm-\rho 1245nm)/(\rho 823nm+\rho 1245nm)$ Landsat = $(\rho 830nm-\rho 2215nm)/(\rho 830nm+\rho 2215nm)$	Landsat, Hyperion
Normalized burn ratio2 (NBR2)*	Hyperion = $(\rho 1245nm-\rho 1649nm)/(\rho 1245nm+\rho 1649nm)$ Landsat = $(\rho 1650nm-\rho 2215nm)/(\rho 1650nm+\rho 2215nm)$	Landsat, Hyperion

Table 1. Vegetation indices calculated using landsat and hyperion/EO-1 data and their respective formulas. References for each formula are available in Appendix S1. *NBR and NBR2 utilize distinct wavelength ranges when measured by the Hyperion and Landsat sensors.

To evaluate the effectiveness of hyperspectral and multispectral VIs in detecting changes in forest disturbance, we first evaluated the eight VIs most sensitive to changes associated with fire, calculated as the maximum difference between burned (B1 year and B3 year) and the Control plot during the fire period, followed by a Linear Model (LM). In these models, we used three variables measured in situ as response variables: biomass, litterfall, and LAI. As predictors, we selected four VIs derived from Landsat (GRND, EVI, NBR, and NDII) and four derived from Hyperion (PRSI, VARI, MSI, and VIG) that were most responsive to changes associated with fire. We present the results for the most sensitive VI derived from Landsat (GRND) and Hyperion (PSRI) in the main text, and the other six VIs are presented in the supplementary information (Figs. S8, S9, and S10).

We also modeled temporal changes in field data (biomass, litterfall, and LAI), as predicted by the VIs most sensitive to fire-related changes. To this end, we applied the loess smoothing method to visualize temporal trends using the *geom_smooth* function in the *ggplot2* R package[23]. Using the differences between the burned and Control treatments for each VI, we estimated the time required for vegetation to recover to the pre-fire baseline values (detailed information is available in Appendix S1: Sect. 1).

Results

Spectral changes in vegetation detected by multispectral VIs

The six Landsat-based VIs indicated a significant reduction in burned area during the prescribed fire period. In contrast, these VIs remained relatively stable in the Control plot (Fig. 2). Prior to our prescribed burns (1985–2004), we observed comparable values for the six VIs between the unburned and burned plots, although the GRND varied more than the other VIs. Following the first experimental fires (2004–2005), reductions in the VIs in the burned plots compared with the Control plots ranged between 3 and 9% for B1 year and 3 and 11% for B3 year. The differences between the burned and Control plots increased as B1 year and B3 year were repeatedly burned. The largest reductions in the studied VIs were observed in 2011, immediately after the least-prescribed burns in 2010, which coincided with a drought event and resulted in high-intensity fires (Fig. 3). After this period, the difference between burned and unburned treatments decreased over time for all VIs, reaching values similar to those of the Control in 2019, nine years after the last fire.

All Landsat-based VIs were sensitive to changes in forest structure, showing similar responses after prescribed burns but varying considerably in magnitude. The VIs that showed the greatest differences relative to the Control were the GRND (87%) and NDII (48%) (Fig. 3). Other Landsat VIs also decreased in the burned plots relative to the Control plot (22% for NBR and EVI, 19% for NBR2, and 14% for NDVI). Confidence intervals confirmed the significance of the observed differences between the burned and Control treatments (Appendix S1, Fig. S1).

Observed differences between the burned plots and the Control were even greater along the forest edges compared with the forest interior for all Landsat VIs. Along the edge, GRND was 200% lower in the B3 year plot

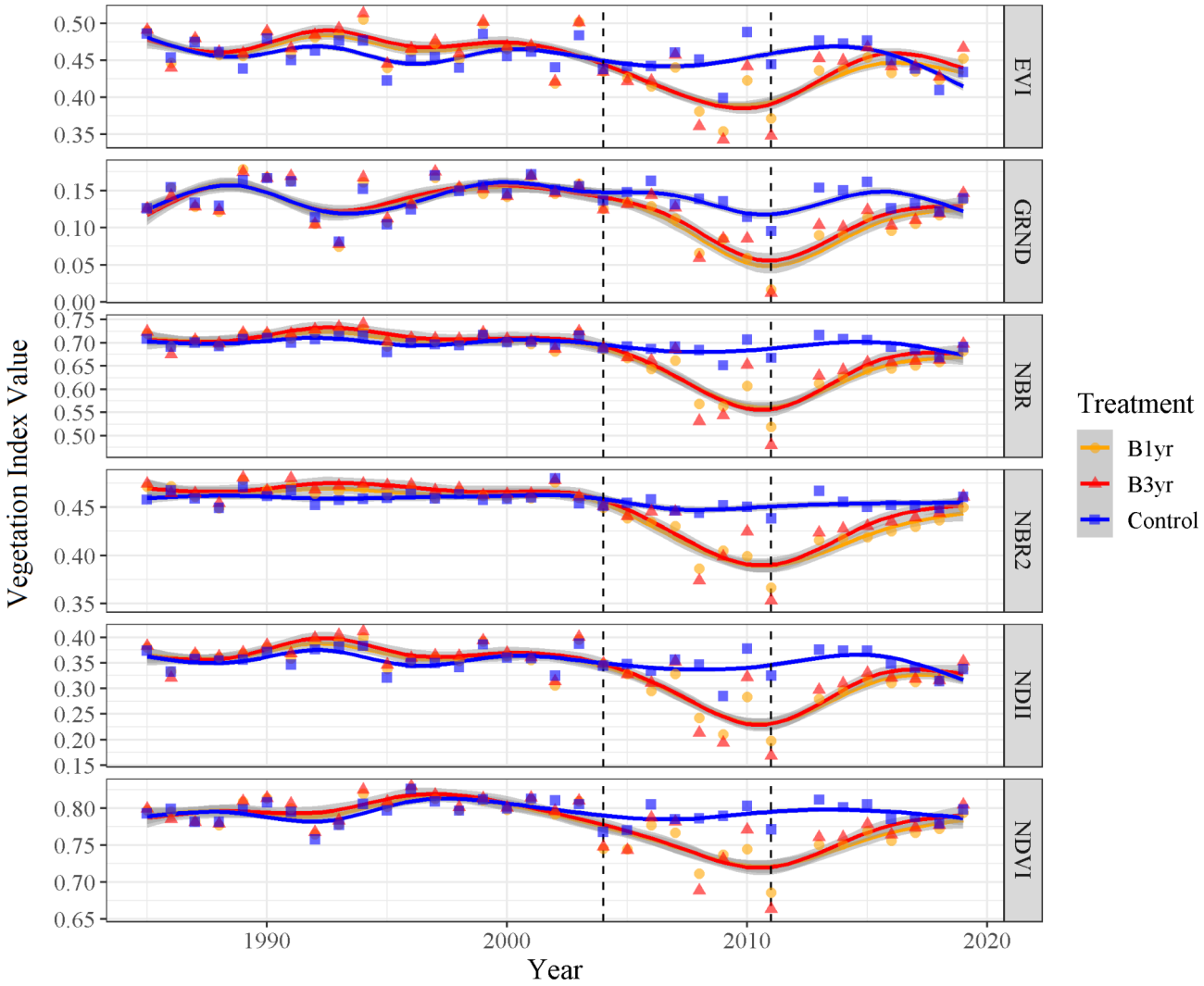

Fig. 2. Temporal patterns of landsat-based vegetation indices (EVI, GRND, NBR, NBR2, NDII, and NDVI) during a fire experiment in southeast Amazonia. Points indicate average values of VIs for the three different fire treatments (Control, B3 year, and B1 year). The dashed vertical lines indicate the period during which the experimental fires occurred (2004 to 2010). The tendency line was generated based on the Loess method, and shading represents the standard error (SE).

than in the Control plot, followed by NDII (102%) and NBR (62%) (Appendix S1, Fig. S2). The forest interior at B3 year exhibited differences of 57% (GRND), 31% (NDII), and 17% (NBR). In contrast, the forest interior of B1 year showed the highest differences, with GRND 66% lower than that of the Control, followed by NDII (32%) and NBR (18%) (Appendix S1: Fig. S3). Although vegetation at the edges showed much higher degradation than in the interior of the plots, the sensitivity patterns among the VIs remained consistent, with the EVI, NBR2, and NDVI capturing smaller differences in both edge and interior vegetation.

After the last experimental fire (2010), the EVI reached values similar to those of the Control plot within four years, recovering quickly compared to other VIs. Other indices reached similar values to the Control plot within five (NDII and NDVI), six (NBR2), or seven years post-fire (GRND and NBR). Along the forest edge, the recovery of VI values took at least two years longer, with EVI and NDVI taking six years to approach baseline values (i.e., prior to the burns), followed by NBR and NDII (seven years), and NBR2 and GRND (eight years) (Appendix S1: Fig. S2). In the case of B3 year, we also observed a recovery of VIs between experimental fires. Between 2007 and 2010, all the VIs returned close to their initial values (Fig. 3 and Appendix S1, Fig. S1).

Efficacy of hyperspectral images for detecting forest degradation

Similar to Landsat, the Hyperion-derived VIs clearly identified forest degradation associated with the experimental fires. The largest differences between the burned and Control plots occurred from 2007 onwards (Fig. 4 and Appendix S1: Fig. S4). Of the 17 VIs evaluated, the greatest differences (>50%) between burned and Control plots were captured by PSRI (94%), VIG (68%), VARI (64%), MSI (56%), and PSSR (54%), all of

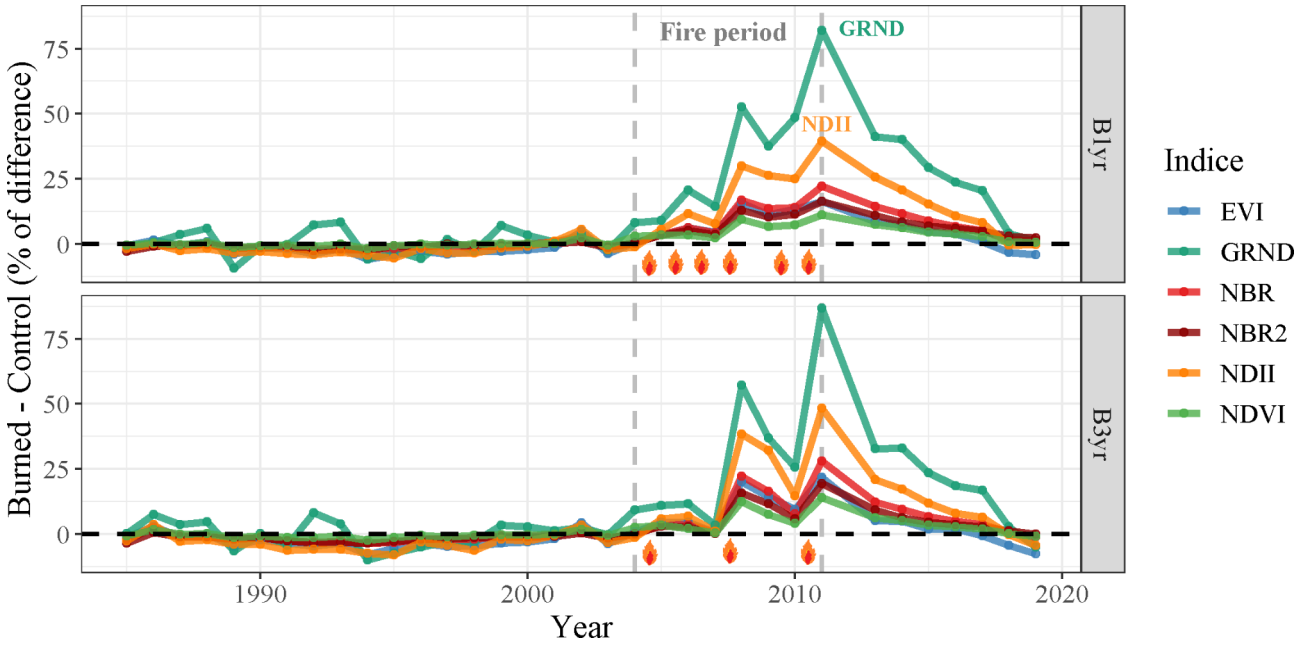

Fig. 3. Relative differences in the spatial means of the multispectral VIs between the unburned control and treatments burned every three years (B3 year) or annually (B1 year). Values indicate the percent change relative to the control. The dashed lines indicate the period during which the fire experiment took place (2004–2010).

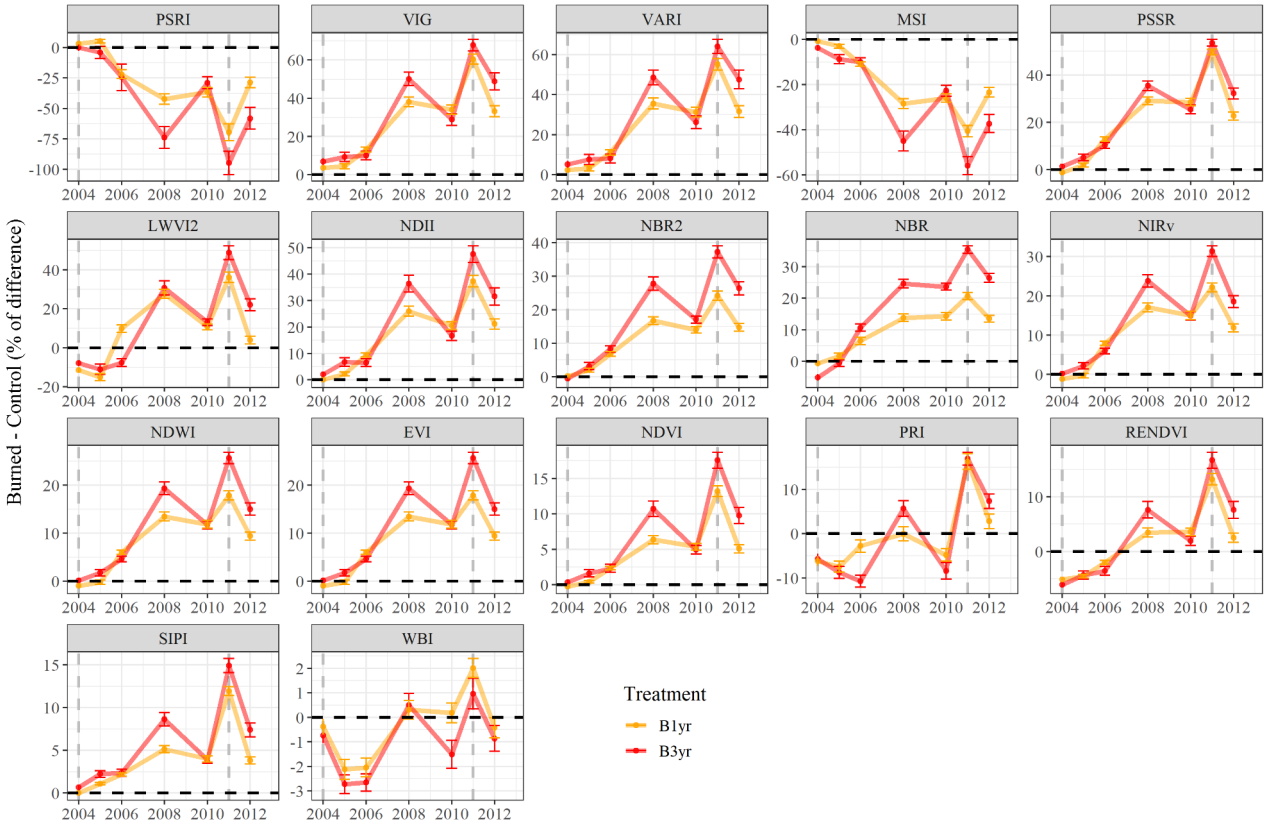

Fig. 4. Relative difference in mean VI values, comparing the unburned Control and treatments burned every three years (B3 year) or annually (B1 year) from 2004–2010. Values indicate the percent change relative to the Control (the horizontal dashed black line), displayed in descending order. Error bars indicate the 95% confidence interval based on the 'Z' test. The vertical dashed lines in gray denote the years of the time period of the prescribed fires (2004–2010).

which are indices associated with vegetation pigmentation or water stress. The VIs that were the least sensitive to degradation by fire were SIPI (15%) and WBI (3%) (Fig. 4).

The differences between the burned and Control plots were greater along the edge (< 250 m) than in the interior (> 250 m) of all Hyperion VIs (Fig. 5). The VIs most responsive to differences between the burned and Control plots showed increasing differences as those plots were burned repeatedly. Similar to the multispectral VIs, the main reductions in hyperspectral VIs occurred between 2007 and 2008 and 2010–2011 (Fig. 5).

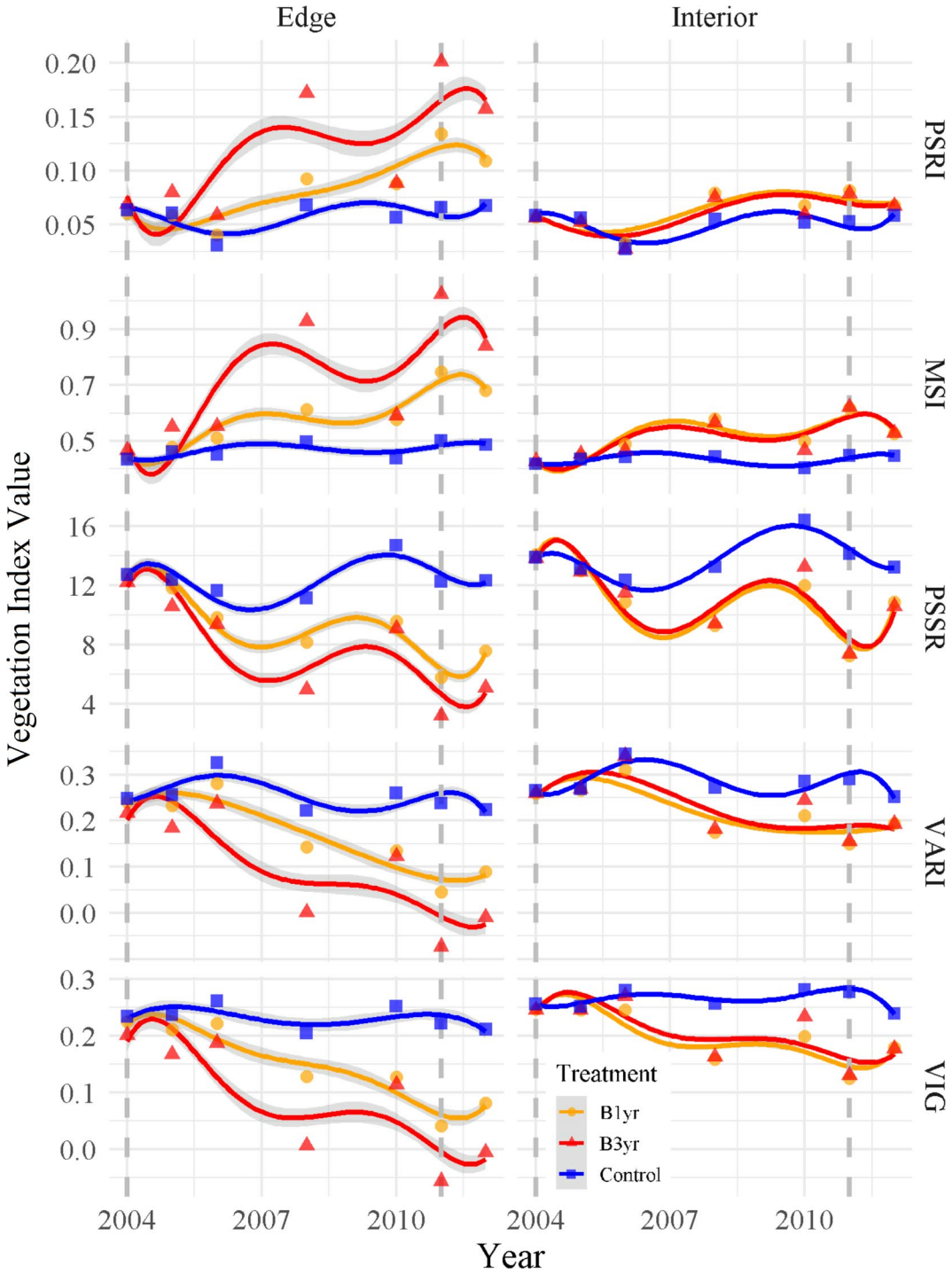

Fig. 5. The temporal patterns of the hyperspectral VIs were more sensitive to changes caused by fire in the experimental plots. The points indicate the average values of the VIs for the three different fire treatments (Control, B3 year, and B1 year). The tendency line was generated based on the loess method, and the shades indicate the standard error (SE). The vertical dashed lines in grey denote the years of the time period of prescribed fires (2004 to 2010).

Vegetation changes detected by hyperspectral vegetation indices

Through analysis of hyperspectral VIs, we identified significant changes and patterns associated with forest fires (Appendix S1, Fig. S5). PCA enabled the identification of clusters of VIs with distinct information patterns (Fig. 6). Although several VIs captured similar responses, others provided unique insights. We observed two main clusters in PC1: The first group represented closed canopies with minor biochemical changes, characterized by NDVI (0.97) and NDII (0.96). The second group was linked to changes in the edges of burned plots, led by PSRI (-0.90) and MSI (-0.97), indicating shifts in vegetation pigmentation and water stress (Appendix S1: Fig. S6). These VIs effectively differentiated treatments over the entire burning period.

Over different study periods, the PCA results varied based on plot conditions, distance from the forest edge, and progression of forest degradation. Most hyperspectral VIs convey similar information owing to their association with similar factors (Appendix S1, Fig. S5). Before the prescribed burns, our PCA analysis indicated

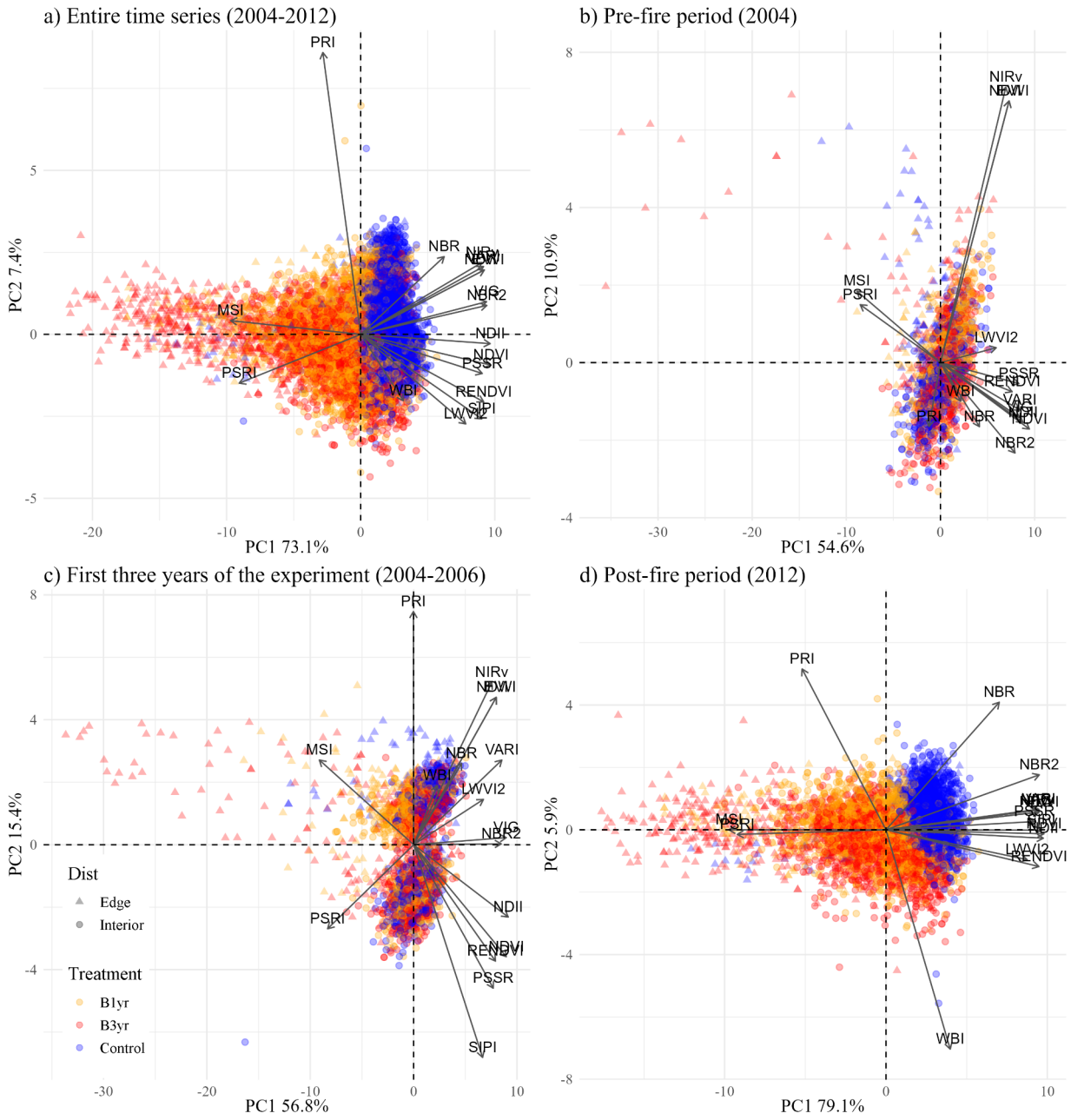

Fig. 6. Projection of the first two principal components from the 17 VIs calculated using Hyperion data for (**a**) the entire time series (2004–2012); (**b**) the pre-fire period; (**c**) the first three years of the experiment (2004–2006); and (**d**) the post-fire period (2012). The results reflect the Control, triennial burning (B3 year), and annual burning (B1 year) treatments, as well as the distance (Dist) from the edge (< 250 m) to the interior (250–1000 m) of the experimental plots. The plots indicate the percentage variance for each component and analysis.

similar characteristics among the treatments, reflecting the initial similarity of the forests during the baseline period. However, modest separation at the treatment edges suggested structural canopy differences (as indicated by clustering of EVI and NIRv) linked to varying vegetation water stress levels (as indicated by MSI and PSRI), which may have predated the fire experiment (Fig. 6b).

The treatments were clearly differentiated after 2007, a year with more intense fires and higher tree mortality, coinciding with distinct VI clusters (Fig. 6c). PCA for each year revealed increasing differences with repeated burns (Appendix S1, Fig. S7). Differences between treatments were primarily associated with PC1, with MSI (-0.97) and PSRI (-0.90) associated with the forest edge, where vegetation was more water-stressed due to prolonged drought (Figs. 4 and 5, and 6d). The NDVI (0.97) and NDII (0.97) tracked a more closed and less stressed canopy cover, as observed in the Control plot, which was concentrated on the right side of PC1 (Fig. 6). Changes related to water stress and vegetation photosynthesis persisted throughout the experiment, as indicated by the PCA results for 2012 (Appendix S1: Fig. S7).

Correlation between hyperspectral and multispectral VIs

Seven of the 17 hyperspectral VIs had a high correlation ($r > +0.8$) with the multispectral VIs (Fig. 7). As expected, the VIs common to the two sensors were the most correlated despite the differences in the spectral resolution in the bands used (wide vs. narrow). These VIs are sensitive to photosynthetic activity and canopy water content, sharing red, NIR, and SWIR spectral bands (VIG, NDWI, NDVI, NDII, NBR2, MSI, NIRv, and EVI). In contrast, the hyperspectral VIs that were least correlated with the multispectral VIs were WBI (also linked to canopy water) and PRI (photosynthesis efficiency). Among the VIs shared by both sensors, NBR had a lower correlation when comparing Hyperion and Landsat ($r = +0.65$). This may be linked to the differences in the formula applied for this index, as it incorporates bands positioned differently within the SWIR range (Table 1).

The Landsat-based GRND (most fire-sensitive multispectral VI) was highly correlated with VARI (+0.91) and VIG (+0.91) from Hyperion. Both VIs were associated with changes in the vegetation pigmentation. VIG is the hyperspectral equivalent of GRND, which also showed a high correlation with PSRI, NIRv, NDWI, NDII, MSI, and EVI (> 0.85). Among the multispectral VIs, GRND had the highest correlation with PSRI ($r = +0.85$). These VIs showed greater sensitivity to changes caused by fire and are associated with vegetation pigmentation.

Capacity of VIs to detect structural changes in burned forests

The experimental fires caused substantial changes in forest litter, LAI, and AGB. Prior to the prescribed fires, no clear differences were observed between the experimental plots (Fig. 8). After the first prescribed fire, all these variables decreased substantially compared to the Control (Fig. 8), especially along the forest edge. For litterfall and LAI, the largest differences between the burned areas and the Control occurred in 2011, when litterfall and LAI were 46% and 69% lower in the burned plots than in the Control, respectively. For AGB, we observed the greatest differences in 2014, when the biomass along the forest edge of the burned plots was 91% lower than that of the Control plot (Fig. 8).

Two years after the end of the prescribed burns, we observed recovery of litterfall and LAI. However, LAI only reached values similar to those of the Control in 2017 (Fig. 8), seven years after the prescribed fires ended. Forest biomass continued to decrease in all burned treatments between 2010 and 2014, when the AGB along the forest edge of B3 year reached 11.9 Mg ha^{-1} (91% lower than that in 2004).

The results showed that the GRND was a better predictor of changes associated with fire than the PSRI (Fig. 9). The capacity of the GRND to detect changes associated with fire was higher for the edge environment than for the forest interior for the tree variables evaluated (Fig. 9). In addition, the explanatory power (R^2) tended to be higher for GRND for the three ground variables (biomass stocks = 0.5–0.8; LAI = 0.8–0.9; litter production = 0.4–0.7), compared to that observed for PSRI (biomass stocks = 0.3–0.8; LAI = 0.6; litter production = 0.3–0.6; Fig. 9).

In general, the other evaluated VIs derived from Landsat (EVI, NBR, and NDII) for the fire period (2004–2011) were consistent with the GRND in predicting litter production, LAI, and biomass stocks (Fig. S8). During the fire recovery period (2011–2017), GRND and NBR produced similar results in predicting biomass, LAI, and litter production (Fig. S9). The other evaluated VIs derived from Hyperion (MSI, VARI, and VIG) for the fire period (2004–2011) were not consistent with the PSRI (Fig. S8). VIG was the best predictor of biomass stocks ($r^2 = 0.7–0.9$), VARI and VIG produced similar results for litter production ($r^2 = 0.4–0.7$) and LAI ($r^2 = 0.7–0.8$; Fig. S8).

Discussion

This study evaluated the sensitivity of hyperspectral and multispectral VIs to changes in forest canopy structure, pigmentation, and function, following disturbances caused by fires and edge effects. The results showed that multispectral VIs are sensitive to short-term changes in vegetation properties after a fire. The most sensitive indices responded to changes in vegetation pigmentation or new foliage (GRND) and shifts in vegetation water content (NDII). Of the set of narrowband VIs measured with Hyperion, the most sensitive was PSRI (followed by NDVI, NDII, and MSI), which was calculated using the red edge at 752 nm, a wavelength outside the range of Landsat's multispectral sensor. Although the VIs assessed here detected most changes in canopy dynamics (e.g., leaf production and LAI), they were less sensitive to changes in the aboveground forest biomass. This study underscores the potential of both hyperspectral and multispectral vegetation indices in detecting forest degradation by fire, and also indicates the hyperspectral bands and VIs that are most effective in assessing the magnitude of changes in vegetation structure and functioning associated with forest fires.

The 17 VIs derived from Hyperion provided more detailed information on biophysical and biochemical changes in the vegetation canopy, despite the shorter time span of sensor imagery. The time series of the Hyperion/

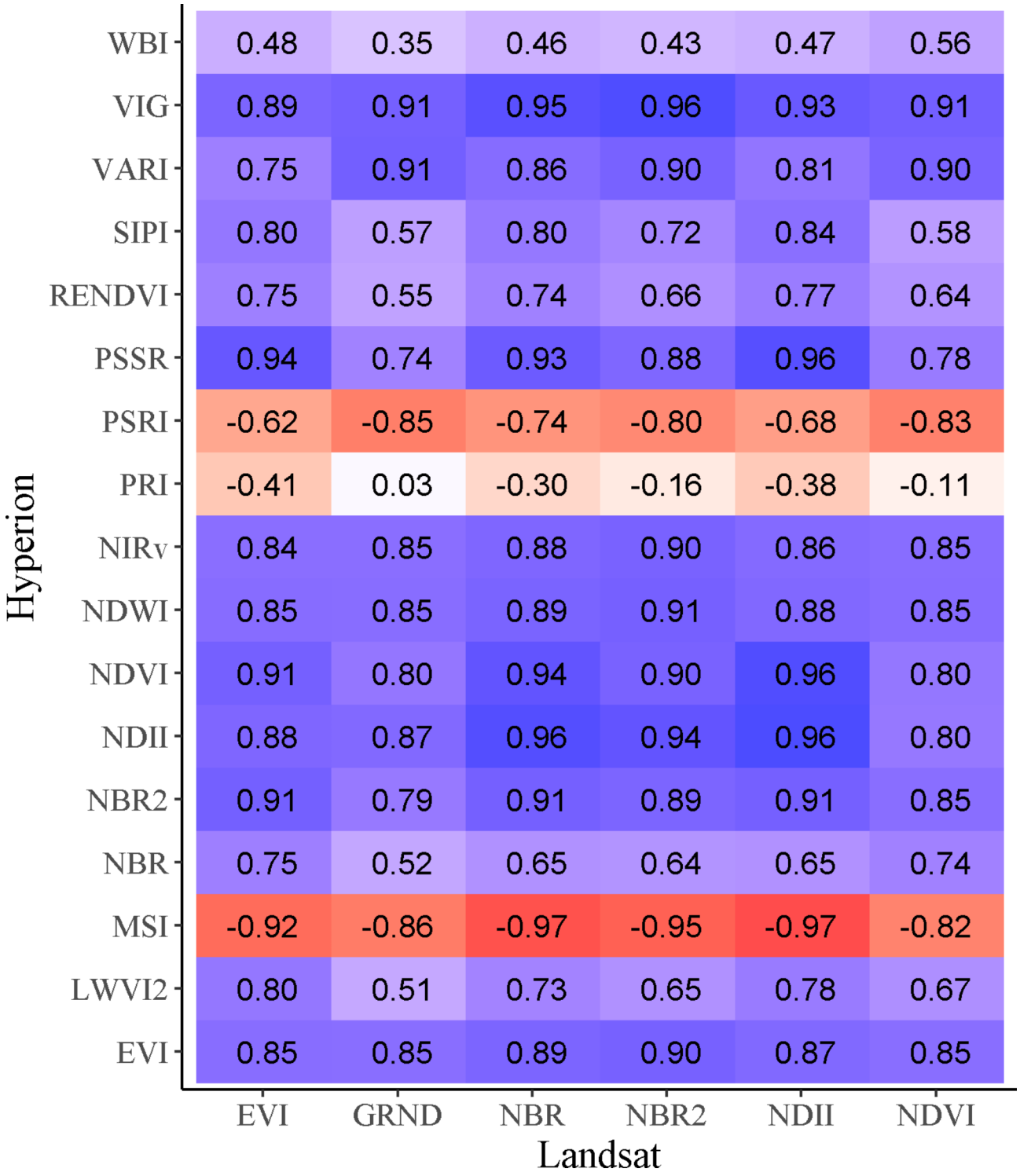

Fig. 7. Pearson's correlation coefficients for the VIs in this study were calculated using hyperion/EO-1 and landsat data.

EO-1 data for the study area was truncated because of operational constraints and significant orbital drift after 2013[25]. Therefore, we were able to assess the efficacy of hyperspectral VIs in capturing forest degradation by fire, but not the regeneration phase. Nevertheless, the Hyperion VIs associated with the ratio of chlorophyll to carotenoids and anthocyanins (e.g., PSRI and PSSR) in vegetation stood out as the most sensitive to vegetation associated with fire, offering an important opportunity to quantify forest degradation[19]. This result is relevant for a new generation of hyperspectral sensors aboard upcoming satellite missions.

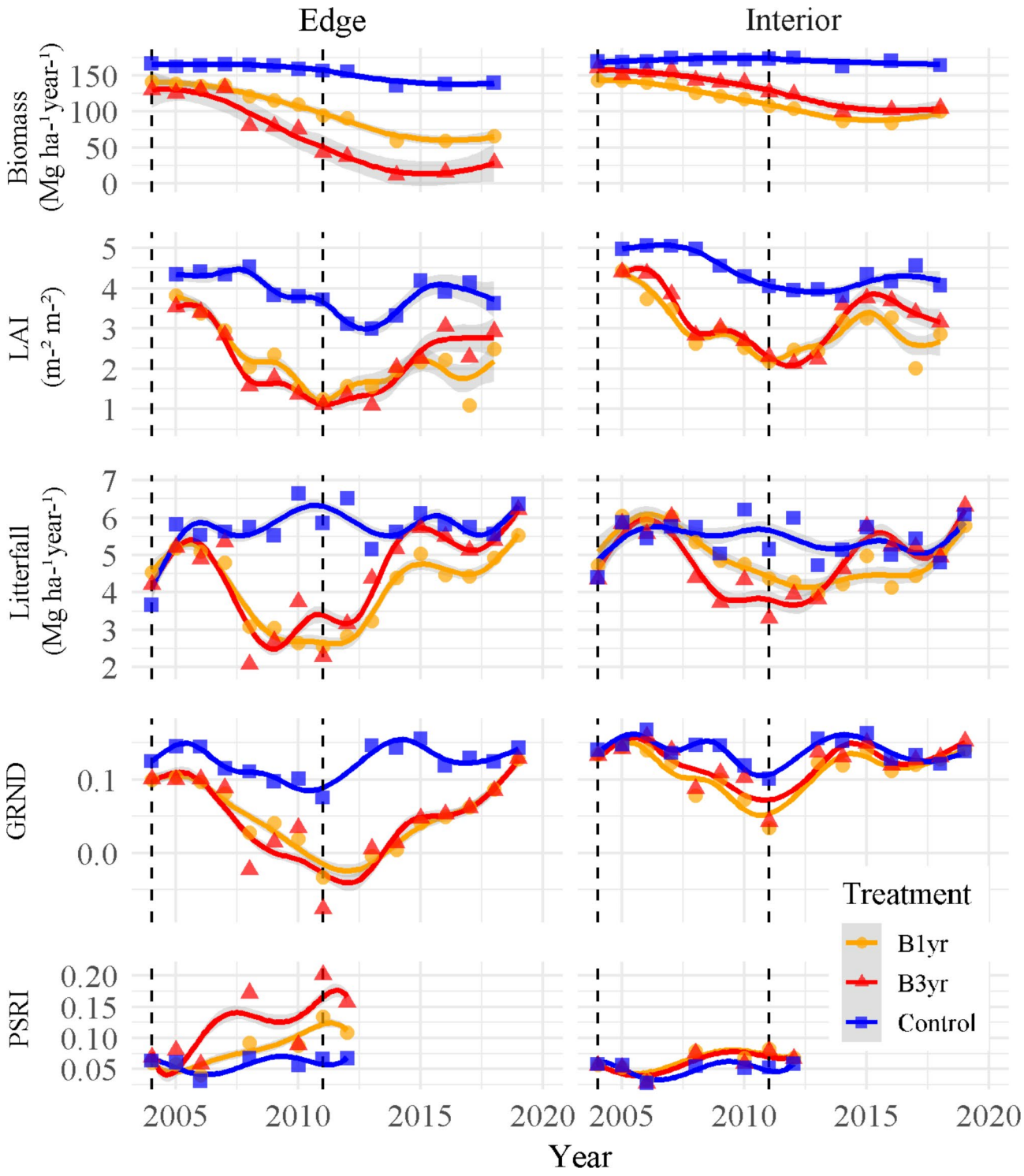

Fig. 8. Temporal patterns of forest structure and productivity (biomass, LAI, and litterfall) based on forest inventories were compared with changes in GRND (Landsat) and PSRI (Hyperion/EO-1) measured along the plot edge and forest interior, as a function of the three experimental treatments (Control, B3 year, and B1 year), where points indicate the average of pixel values for each treatment. The tendency line was generated based on loess method and the shades indicates the standard error (SE). The vertical dashed lines denote the period of the prescribed fires (2004–2010).

Hyperspectral VIs calculated based on Hyperion can be classified into two broad categories. The first includes indices that are sensitive to small biochemical changes related to photosynthesis, pigmentation (NDVI, RENDVI, VARI, and VIG), and canopy water content (NDWI, NDII, and LWVI2). The second group (PSRI and MSI) captures changes at the edge of burned forests and the signals associated with vegetation stress[25]. Our

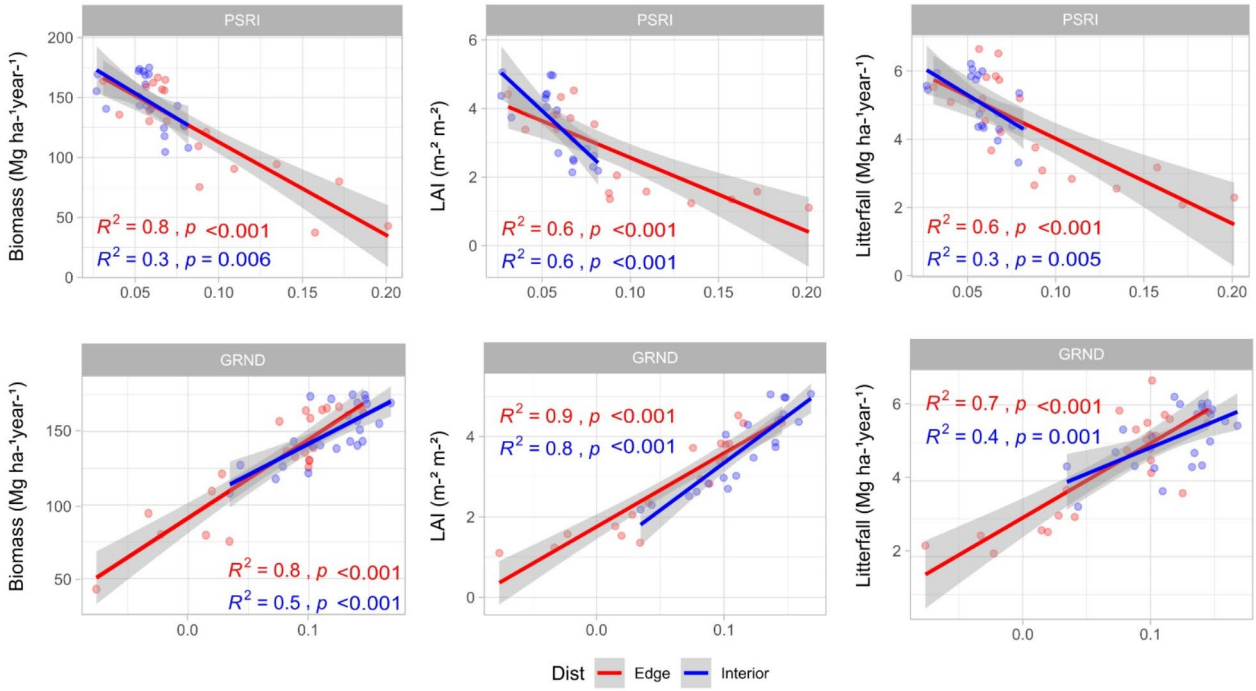

Fig. 9. The linear model for the period during fire events (2005–2011) using as response the three forest structure and productivity variables measured in the field (biomass, LAI, and litterfall) as a function or GRND (Landsat) and PSRI (Hyperion/EO-1). For this analysis, response variables and VIS were measured along the plot edge (0–250 m; in red) and forest interior (250–1000 m; in blue), and information on the two burned areas (B3 year and B1 year) were included in the same analysis.

PCA indicated that NDVI, NDII, PSRI, and MSI are most useful for detecting vegetation degradation. NDVI is widely used and relates to chlorophyll content by analyzing the differences in NIR and red reflectance[26,27]. NDII is positively correlated with canopy water content by taking the normalized difference between NIR and SWIR-1[28], whereas MSI is negatively correlated with canopy water, given that it is calculated by dividing SWIR-1 by NIR[29]. Finally, PSRI is sensitive to changes in vegetation pigmentation, particularly the chlorophyll/carotenoid ratio, which can indicate senescence[30,31].

In general, the VIs values for the forest interior were similar across experimental plots during the pre-fire period. However, the same VIs proved useful in detecting forest degradation caused by edge effects. PSRI and MSI revealed different spectral signatures at the plot borders, indicating vegetation stress along forest edges (Fig. 6a). This suggests that the more severe fire effects observed at plot borders may be linked to vegetation stress and edge effects that predate the fire experiment. After the first experimental fires, PSRI and MSI detected substantial changes at the forest edge in treatments B1 year and B3 year and smaller changes within the burned forests compared to the Control.

After two consecutive fire events, LWVI2 and RENDVI detected changes in the experimental area that were not captured by multispectral VIs, indicating their sensitivity to small changes in canopy foliage content, canopy opening fraction, and senescence[32]. These results indicate that VIs using the red-edge spectral range may be more sensitive to degradation caused by early or low-intensity fires. Moreover, LWVI2 uses bands at 1094 and 1205 nm, which are sensitive to leaf and canopy water, respectively[33]. This suggests that the first (spectral) degradation signals may indicate increased water stress in the vegetation.

Higher changes in VIs values for the burned plots were observed after intense fires associated with more severe drought conditions. Few VIs detected changes in forest structure and biochemistry after the first two fire events in the B1 year plot and after one fire event in the B3 year plot (i.e., prior to 2007). PSRI (Hyperion) and GRND (Landsat) showed modest changes (> 15%) in the treatment plots compared to the Control, but all other VIs failed to capture significant differences. After the high-intensity fires during the 2007 drought, when fuel loads were increased and understory humidity lower[1,34], the differences between burned plots and the Control increased for all VIs. After 2007, there were large reductions in LAI and litterfall and a sharp drop in biomass – detected by most VIs, especially those sensitive to water stress and vegetation pigmentation (e.g., GRND and NDII from Landsat; PSRI, VIG, VARI, MSI, and PSSR from Hyperion). These results confirm that near-infrared and shortwave infrared bands, already known for their effectiveness, are crucial for detecting fire-induced degradation dynamics, supporting their continued use in existing satellite-based fire indices.

Our results during the post-fire recovery period show that the signal of forest degradation disappears quickly, even after repeated burns. All VIs in the burned plots reached values close to those observed in the Control plot within eight years. The recovery of multispectral VIs reflects the recovery of photosynthetic capacity and

structure (e.g., EVI, NDVI, and GRND)[35], as well as canopy water conditions (NDII). These changes can be interpreted as a decrease in water stress compared to years when forests still suffered from repeated fires. This is consistent with previous work using eddy covariance measurements, which showed a rapid recovery of CO_2 and H_2O fluxes in burned plots[7]. The authors of that study concluded that the effects of fire extended 3.5 years into the recovery period, which can be associated with recovery of the EVI, NDVI, and NDII signals. Regeneration was also detected in the recovery of NBR and NBR2, which showed fire scars disappearing from the landscape over time.

The recovery of the hydrological and carbon cycles, measured in the field and reflected by the VIs, could lead to misinterpretation of satellite-based forest recovery metrics. Our results show that VIs reflect changes in canopy leaf production dynamics, but are not sensitive to changes in forest biomass. The recovery of canopy productivity is insufficient to compensate for biomass losses from the increased mortality of large trees, a process that can take several decades[36]. Moreover, the forest degradation process does not end with the last fire event because subsequent disturbances can amplify forest degradation. Windstorms, for example, can increase the degradation of burned forests and delay biomass recovery, particularly because fires weaken tree trunks and make them more vulnerable to snapping under strong winds[37].

In summary, the recovery of VI values does not necessarily represent the recovery of biomass or the return of forests to their pre-experimental ecological state. In fact, they may represent the beginning of ecological succession led by pioneer species after forest degradation[4]. There was an increase in grass invasion and recruitment of pioneers throughout the experimental area during the regeneration period[7,37–39]. Pioneer species invest in rapid growth and tend to exhibit lower water-use efficiency[40], which is reflected in the VIs linked to photosynthesis, water, and greening. Although these VIs do not accurately capture the structural recovery of forests, they do provide important information on the capacity of forests to recover critical ecosystem services linked to carbon and hydrological cycles[41].

Final considerations

Both Landsat (TM and OLI) and Hyperion/EO-1 detected forest degradation associated with the experimental fires. However, hyperspectral VIs provide higher sensitivity and a greater range of information regarding degradation, thus increasing our ability to detect and characterize disturbances. PSRI accurately represents the processes of vegetation senescence and is the VI with the highest sensitivity to edge effects. Hyperspectral VIs associated with carotenoid/chlorophyll and multispectral indices linked to pigmentation and new foliage (e.g., GRND) were the first to detect water stress and vegetation degradation associated with forest fires. Further research on indices capable of detecting early changes in these variables could advance fire-risk mapping. Despite the recovery of multispectral VI values and litter production post-fire, there are still important legacies of fires (e.g. AGB, vegetation structure, and composition) that are masked by the rapid growth of pioneers and invasive grasses, reflected in increasing VI values.

Data availability

The data that supports the findings of this study are available from the corresponding author upon reasonable request.

Received: 21 June 2024; Accepted: 28 October 2024
Published online: 08 November 2024

References

1. Brando, P. M. et al. Abrupt increases in amazonian tree mortality due to drought–fire interactions. *Proc. Natl. Acad. Sci. USA*. **111**, 6347–6352 (2014).
2. Lapola, D. M. et al. The drivers and impacts of Amazon forest degradation. *Science*. **379**, eabp8622 (2023).
3. Gatti, L. V. et al. Drought sensitivity of amazonian carbon balance revealed by atmospheric measurements. *Nature*. **506**, 76–80 (2014).
4. Prestes, N. C. C. D. S. et al. Fire effects on understory forest regeneration in Southern Amazonia. *Front. Glob. Chang.*. **3**, 10 (2020).
5. Brando, P. M. et al. The gathering firestorm in southern Amazonia. *Sci. Adv.* **6**, eaay1632 (2020).
6. Asner, G. P., Nepstad, D., Cardinot, G. & Ray, D. Drought stress and carbon uptake in an Amazon forest measured with spaceborne imaging spectroscopy. *Proc. Natl. Acad. Sci. USA* **101**, 6039–6044 (2004).
7. Brando, P. M. et al. Prolonged tropical forest degradation due to compounding disturbances: Implications for CO_2 and H_2O fluxes. *Glob. Chang. Biol.* **25**, 2855–2868 (2019).
8. Coe, M. T. et al. Deforestation and climate feedbacks threaten the ecological integrity of south–southeastern Amazonia. *Phil Trans. R. Soc. B*. **368**, 20120155 (2013).
9. Nepstad, D. et al. Amazon drought and its implications for forest flammability and tree growth: A basin-wide analysis: Amazon drought and forest flammability. *Glob. Chang. Biol.* **10**, 704–717 (2004).
10. Matricardi, E. A. T. et al. Long-term forest degradation surpasses deforestation in the Brazilian Amazon. *Science*. **369**, 1378–1382 (2020).
11. Shimabukuro, Y. E. et al. Monitoring deforestation and forest degradation using multi-temporal fraction images derived from Landsat sensor data in the Brazilian Amazon. *Int. J. Remote Sens.* **40**, 5475–5496 (2019).
12. Sasaki, N. & Putz, F. E. Critical need for new definitions of forest and forest degradation in global climate change agreements. *Conserv. Lett.* **2**, 226–232 (2009).
13. Numata, I., Cochrane, M. A. & Galvão, L. S. Analyzing the impacts of frequency and severity of forest fire on the recovery of disturbed forest using landsat time series and EO-1 hyperion in the Southern Brazilian Amazon. *Earth Interact.* **15**, 1–17 (2011).
14. Jarchow, C. J., Nagler, P. L. & Glenn, E. P. Greenup and evapotranspiration following the minute 319 pulse flow to Mexico: An analysis using landsat 8 normalized difference vegetation index (NDVI) data. *Ecol. Eng.* **106**, 776–783 (2017).
15. Wilson, N. R. & Norman, L. M. Analysis of vegetation recovery surrounding a restored wetland using the normalized difference infrared index (NDII) and normalized difference vegetation index (NDVI). *Int. J. Remote Sens.* **39**, 3243–3274 (2018).
16. Shimabukuro, Y. E. et al. Mapping burned areas of Mato Grosso State Brazilian Amazon using multisensor datasets. *Remote Sens.* **12**, 3827 (2020).

17. Flores, B. M. et al. Critical transitions in the Amazon forest system. *Nature*. **626**, 555–564 (2024).
18. Asner, G. P. et al. Selective logging in the Brazilian Amazon. *Science*. **310**, 480–482 (2005).
19. Jacon, A. D., Galvão, L. S., Santos, D., Sano, E. E. & J. R. & Seasonal characterization and discrimination of Savannah physiognomies in Brazil using hyperspectral metrics from Hyperion/EO-1. *Int. J. Remote Sens.* **38**, 4494–4516 (2017).
20. Balch, J. R. K. et al. Negative fire feedback in a transitional forest of southeastern Amazonia. *Glob. Chang. Biol.* **14**, 2276–2287 (2008).
21. Alvares, C. A., Stape, J. L., Sentelhas, P. C., De Moraes Gonçalves, J. L. & Sparovek, G. Köppen's climate classification map for Brazil. *metz.* **22**, 711–728 (2013).
22. Brando, P. M. et al. Legacies of multiple disturbances on fruit and seed patterns in Amazonia: Implications for forest functional traits. *Ecosphere*. **15**, e4780 (2024).
23. Wickham, H. Getting Started with ggplot2. in *ggplot2*, 11–31. (Springer International Publishing, Cham, 2016). https://doi.org/10.1007/978-3-319-24277-4_2
24. Cleveland, W. S. & Devlin, S. J. Locally weighted regression: An approach to regression analysis by local fitting. *J. Am. Stat. Assoc.* **83**, 596–610 (1988).
25. Galvão, L. S., De Souza, A., Breunig, F. M. & A. & A hyperspectral experiment over tropical forests based on the EO-1 orbit change and PROSAIL simulation. *GIScience Remote Sens.* **57**, 74–90 (2020).
26. Hatfield, J. L., Asrar, G. & Kanemasu, E. T. Intercepted photosynthetically active radiation estimated by spectral reflectance. *Remote Sens. Environ.* **14**, 65–75 (1984).
27. Rouse, W., Haas, R. H. & Deering, W. MONITORING THE VERNAL ADVANCEMENT AND RETROGRADATION (GREEN WAVE EFFECT) OF NATURAL VEGETATION.
28. Hardisky, M. A., Klemas, V. & Smart, R. M. The influence of soil salinity, growth form, and leaf moisture on the spectral radiance of Spartina alterniflora canopies. *Photogramm Eng. Remote Sens.* **49**, 77–83 (1983).
29. Huntjr, E. & Rock, B. Detection of changes in leaf water content using Near- and middle-infrared reflectances☆. *Remote Sens. Environ.* **30**, 43–54 (1989).
30. Galvão, L. S., Roberts, D. A., Formaggio, A. R., Numata, I. & Breunig, F. M. View angle effects on the discrimination of soybean varieties and on the relationships between vegetation indices and yield using off-nadir Hyperion data. *Remote Sens. Environ.* **113**, 846–856 (2009).
31. Merzlyak, M. N., Gitelson, A. A., Chivkunova, O. B. & Rakitin, V. Y. U. Non-destructive optical detection of pigment changes during leaf senescence and fruit ripening. *Physiol. Plant.* **106**, 135–141 (1999).
32. Gitelson, A. A., Merzlyak, M. N. & Lichtenthaler, H. K. Detection of red edge position and chlorophyll content by reflectance measurements near 700 nm. *J. Plant Physiol.* **148**, 501–508 (1996).
33. Galvão, L. S., Formaggio, A. R. & Tisot, D. A. Discrimination of sugarcane varieties in Southeastern Brazil with EO-1 Hyperion data. *Remote Sens. Environ.* **94**, 523–534 (2005).
34. Balch, J. K. et al. Size, species, and fire behavior predict tree and liana mortality from experimental burns in the Brazilian Amazon. *For. Ecol. Manag.* **261**, 68–77 (2011).
35. de Moura, Y. M. et al. Spectral analysis of amazon canopy phenology during the dry season using a tower hyperspectral camera and modis observations. *ISPRS J. Photogramm. Remote Sens.* **131**, 52–64 (2017).
36. Silva, S. S. D. et al. Dynamics of forest fires in the southwestern Amazon. *For. Ecol. Manag.* **424**, 312–322 (2018).
37. Silvério, D. V. et al. Fire, fragmentation, and windstorms: A recipe for tropical forest degradation. *J. Ecol.* **107**, 656–667 (2019).
38. Brando, P. M. et al. Fire-induced tree mortality in a neotropical forest: The roles of bark traits, tree size, wood density and fire behavior. *Glob. Chang. Biol.* **18**, 630–641 (2012).
39. Silvério, D. V. et al. Testing the Amazon savannization hypothesis: Fire effects on invasion of a neotropical forest by native cerrado and exotic pasture grasses. *Phil Trans. R Soc. B*. **368**, 20120427 (2013).
40. Nogueira, A., Martinez, C. A., Ferreira, L. L. & Prado, C. H. B. A. Photosynthesis and water use efficiency in twenty tropical tree species of differing succession status in a Brazilian reforestation. *Photosynt*. **42**, 351–356 (2004).
41. Bonan, G. B. Forests and climate change: Forcings, feedbacks, and the climate benefits of forests. *Science*. **320**, 1444–1449 (2008).

Acknowledgements

We thank Ricardo Dalagnol, Sami Rifai, and Ana Freitas for their help in processing satellite images. We also thank Andreia Ribeiro and Bianca Rebelatto for providing thoughtful comments that have improved this manuscript. The outstanding field research team of the Amazon Environmental Research Institute (IPAM) assisted with fieldwork and logistics at the Tanguro field site. The INPE provided logistical support and expertise in processing multispectral and hyperspectral satellite data. The University of Mato Grosso State in Nova Xavantina (UNEMAT) has provided vital infrastructure and support.

Author contributions

E. Q. M., D. V. S. and P. M.: Writing the main manuscript text. E. Q. M., D. V. S., L. S. G., L. E. O. C. A., P. M. B.: Conceptualization, Methodology, Writing. M. R. U., M. N. M., L. R. and A. A. C. A.: Revising the manuscript, Writing.

Funding

This work was funded by NASA's Carbon Monitoring System (CMS) (#80NSSC21K01435) and the Interdisciplinary Research in Earth Science (IDS) (#80NSSC24K0301) programs, the National Science Foundation (NSF) (#2325993), the Coordenação de Aperfeiçoamento de Pessoal de Nível Superior – Brasil (CAPES) (Finance Code 001), the CAPES PDPG program (#88887.691425/2022.00), and Fundação de Amparo à Pesquisa do Estado de São Paulo (FAPESP) (#2023/03965-9) and Conselho Nacional de Desenvolvimento Científico e Tecnologico (Research fellowship PQ2 #311468/2022-5).

Declarations

Competing interests

The authors declare no competing interests.

Additional information

Supplementary Information The online version contains supplementary material available at https://doi.org/1

0.1038/s41598-024-77924-3.

Correspondence and requests for materials should be addressed to E.Q.M.